Spatial imaging of proton via leading-twist nonskewed GPDs with basis light-front quantization

Satvir Kaur,[*] Siqi Xu,[†] Chandan Mondal,[‡] and Xingbo Zhao[§]

Institute of Modern Physics, Chinese Academy of Sciences, Lanzhou 730000, China;
School of Nuclear Science and Technology, University of Chinese Academy of Sciences,
Beijing 100049, China;
and CAS Key Laboratory of High Precision Nuclear Spectroscopy, Institute of Modern Physics,
Chinese Academy of Sciences, Lanzhou 730000, China

James P. Vary[‖]

Department of Physics and Astronomy, Iowa State University, Ames, Iowa 50011, USA

(BLFQ Collaboration)

The internal image of the proton is unveiled by examining the generalized parton distributions (GPDs) at zero skewness, within the basis light-front quantized environment. Several distributions emerge when a quark is sampled with different currents depending upon the helicity arrangements of the active quark and the proton target. We investigate six of the eight leading-twist proton GPDs of the valence quarks, the helicity conserving distributions $(H, E, \tilde{H})$ and the helicity nonconserving $(H_T, E_T, \tilde{H}_T)$ distributions at skewness set to zero $(\zeta = 0)$. We consider purely transverse momentum transfer and, hence, obtain results describe only the proton's two-dimensional structure in the transverse plane. We present the Mellin moments of these distribution functions, where the first moment produces a form factor and the second Mellin moments help extract the information on partonic contributions to the hadronic angular momentum. We compare our results for the Mellin moments with those from lattice QCD and other approaches where available. We also present the GPDs in transverse position space.

I. INTRODUCTION

Probing the hadron's complex internal structure provides knowledge of the nonperturbative aspects of quantum chromodynamics (QCD) and insights into fundamental questions such as the nature of confinement. Generalized parton distributions (GPDs) are three-dimensional functions that convey structural details of the hadron. For example, from these functions, one can obtain information about the distribution of partons in the plane transverse to the direction in which the hadron is moving. Alternatively, one can deduce the distribution of the longitudinal momentum carried by the partons. These distribution functions have the potential to address one of the major issues in hadron physics—the proton spin problem. This is simply because the GPDs provide information on the orbital motion of the partons in conjunction with their spatial flavor distributions.

Multivariable GPDs are functions of (x, ζ, t) where x is the longitudinal momentum fraction held by the parton, while $\zeta(= -\Delta^+/2P^+)$ and $t(= \Delta^2)$ define the longitudinal momentum transfer from the initial to the final state of a hadron and the square of the total momentum transferred, respectively. While they are not probabilistic functions, their two-dimensional (2D) Fourier transforms from transverse momentum transfer to the impact-parameter plane in the absence of the longitudinal momentum transfer provide a probabilistic interpretation of the GPDs [1,2].

Further value can be derived from GPDs by implementing certain limits that provide notable 1D distributions. For instance, the first Mellin moments of different GPDs reproduce different form factors depending upon the helicity configurations of both quark and proton.

[*]satvir@impcas.ac.cn
[†]xsq234@impcas.ac.cn
[‡]mondal@impcas.ac.cn
[§]xbzhao@impcas.ac.cn
[‖]jvary@iastate.edu

Also, one can retrieve the parton distribution functions (PDFs) at the forward limit of the GPDs, i.e. when there is no momentum transfer from the initial to the final state of the proton. Further, at the $t \to 0$ limit, one can find the connection of GPDs via second Mellin moments to the quark's and gluon's angular momentum distribution inside the hadron. An indirect connection has been stated between the basic mechanical properties of the proton, like pressure, shear distributions etc. and the GPDs [3]. It is worth noticing that the different helicity configurations of the active parton and the hadron give rise to different GPDs and they, in turn, provide a bounty of information on the hadron structure and its spin.

The GPDs are generally classified into two categories: the chiral-even GPDs and the chiral-odd GPDs based on whether the quark helicity is preserved or not. At leading twist, the chiral-even GPDs are further divided into unpolarized $[H(x,\zeta,t), E(x,\zeta,t)]$ and helicity-dependent GPDs $[\tilde{H}(x,\zeta,t), \tilde{E}(x,\zeta,t)]$, where H and $\tilde{H}$ appear when the helicity of the proton is conserved in the initial and final states, which is not the case for E and $\tilde{E}$. The GPD $\tilde{E}$ can be evaluated by considering the momentum transfer in the longitudinal direction. Since we focus on extracting the GPDs at $\zeta = 0$, $\tilde{E}$ is beyond the scope of this work. To clarify, one can potentially determine $\tilde{E}$ by conducting a calculation at a nonzero ζ value in order to isolate this GPD from the parametrization. Then, substituting $\zeta = 0$ may provide the nonzero distribution. Hence, the approach used in this study initializes ζ as zero at the outset of the calculation, making $\tilde{E}$ unattainable using this approach. These GPDs are convoluted with other quantities when forming representations of amplitudes for hard exclusive processes, such as deeply virtual Compton scattering [4–6] and deeply virtual meson production [7].

Extensive experimental efforts have been undertaken to investigate GPDs. One can cite, for example, H1 [8,9], ZEUS [10,11], HERMES at DESY [12–14], Hall A [15,16], CLAS at Jefferson Lab [17–19], COMPASS at CERN [20]. Recently, these distributions have been determined by analysing the world electron scattering data [21,22].

There are a total of four chiral-odd GPDs, also known as transversity GPDs: $H_T(x,\zeta,t)$, $E_T(x,\zeta,t)$, $\tilde{H}_T(x,\zeta,t)$, and $\tilde{E}_T(x,\zeta,t)$. The distribution $\tilde{E}_T$ vanishes for $\zeta = 0$, since it is an odd function under the transformation $\zeta \to -\zeta$. Such GPDs are quite challenging to measure through hard exclusive processes. Nevertheless, it has been proposed that these GPDs could be probed in diffractive double meson electroproduction [23–25]. Theoretical efforts have shown the possibility of describing the hard exclusive electroproduction of pseudoscalar mesons by a hard scattering mechanism involving the leading-twist chiral-odd GPDs of the nucleon [26–31]. The first evidence of the existence of these GPDs was given by the COMPASS collaboration where the exclusive production of ρ^0 mesons was studied by scattering muons off transversely polarized

protons [32]. Results from GPDs-based model calculations were found to be in agreement with the data. Further, results of exclusive π^0 and η electroproduction by CLAS collaboration confirm the direct experimental accessibility of transversity GPDs [33,34]. It is noteworthy that experiments are planned to extract GPDs at upcoming facilities such as the Electron Ion Collider [35], the Electron Ion Collider in China [36,37] and the 12 GeV upgrade program at Jefferson Lab [38,39].

Theoretically, the proton GPDs have drawn immense attention. Several QCD inspired models have been developed to understand the proton structure (see, for example, Refs. [40–52]), but deriving the theoretical links with QCD remains a challenge. For instance, numerous studies on moments which are related to the GPDs in certain limits are presented in the lattice QCD approach [53–60] and Dyson-Schwinger equation approach [61–64]. Unlike the Euclidean methods, the QCD observables are directly obtainable in Minkowski space-time. However, no such method has been developed so far. The basis light-front quantization (BLFQ) approach [65–72] has potential to achieve this goal of solving the QCD from first principles when QCD interactions alone are included. Since we consider only the valence Fock sector, this work utilizes an effective Hamiltonian, in essence a QCD-inspired model, in order to solve for observables.

We adopt the BLFQ approach which is a convenient framework defined on the light-front to get the hadron spectra and its structure while obtaining the light-front wave functions (LFWFs) through diagonalization of the Hamiltonian. One can access the distributions of sea quarks and gluons in this approach by including the higher Fock sector representations of a hadron. This approach has successfully described the QCD bound states of mesons [68,69,73–79] and baryons [70,71,80–82]. Recently, these states have been expanded in the Fock space including one dynamical gluon component for the pion $|q\bar{q}g\rangle$ [79] and the nucleon $|qqqg\rangle$ [83]. Within this approach, one now has access to the gluon distributions based on coupling defined by QCD.

In this work, we employ the LFWFs to study the proton GPDs by taking into account the valence Fock sector $|qqq\rangle$, where the chiral-even GPDs along with the other applications have already been studied [70,71,80]. Note that the proton form factors (FFs), such as electromagnetic FFs and axial-vector FFs have been evaluated in this approach and have been found consistent with the available experimental data [70,71]. Further, the 1D proton PDFs, particularly the unpolarized, helicity-dependent and transversity PDFs have been examined by comparing them with the available global fits and measured data [70,71]. Overall, the results have been found in agreement with the data. In Ref. [80], the angular momentum distributions have been explored, which have been evaluated using the unpolarized and helicity-dependent GPDs. The previous results are

encouraging and motivate us to extend this approach to study the chiral-odd GPDs, when the quark helicity flips unlike for the case of chiral-even GPDs. The 3D chiral-odd GPDs are the extended version of the transversity PDF and tensor form factors, which provide the spatial tomography of the proton when the valence quarks are transversely polarized. In this way, the chiral-odd GPDs provide important details on the correlation between the angular momentum and spin of quarks inside the proton.

Our aim is to investigate the structure of the proton through its GPDs and other observables in greater detail in order to provide a better understanding using the BLFQ approach. Our selected observables include different Mellin moments (so-called generalized form factors) and impact-parameter dependent GPDs.

II. BASIS LIGHT-FRONT QUANTIZATION APPROACH

In the BLFQ approach, an eigenvalue problem of the Hamiltonian, $H_{\text{eff}}|\Psi\rangle = M_H^2|\Psi\rangle$, is solved on the light front (LF). The eigensolutions provide LFWFs, and the eigenvalues are recognized as the hadronic mass spectra (M_H). The former play crucial roles in understanding the detailed structure of QCD bound state systems.

The baryonic state on which the Hamiltonian operator would act is expanded at fixed LF time as

$$|\Psi\rangle = \psi_{(qqq)}|qqq\rangle + \psi_{(qqq\bar{q})}|qqq\bar{q}\rangle \\ + \psi_{(qqqg)}|qqqg\rangle + \cdots, \tag{1}$$

where q, $\bar{q}$, and g represent quark, antiquark, and gluon Fock particles, respectively. The significance of LFWFs $\psi_{(qqq)}, \psi_{(qqq\bar{q})}, \psi_{(qqqg)}, \ldots$ is to provide the probability amplitudes for the Fock states defined by $|qqq\rangle$, $|qqq\bar{q}\rangle$, $|qqqg\rangle$ and so on. In this work, we consider only the valence Fock state, i.e., the first term in Eq. (1).

The effective Hamiltonian of the baryonic systems in our chosen Fock space is defined as [70,71,80–82]

$$H_{\text{eff}} = \sum_i \frac{\mathbf{k}_{\perp i}^2 + m_i^2}{x_i} \\ + \frac{1}{2}\sum_{i \neq j} \kappa^4 \left(x_i x_j (\mathbf{r}_{\perp i} - \mathbf{r}_{\perp j})^2 - \frac{\partial_{x_i}(x_i x_j \partial_{x_j})}{(m_i + m_j)^2} \right) \\ + \frac{1}{2}\sum_{i \neq j} \frac{4\pi C_F \alpha_s}{Q_{ij}^2} \bar{u}_{s_i'}(k_i')\gamma^\mu u_{s_i}(k_i)\bar{u}_{s_j'}(k_j')\gamma^\nu u_{s_j}(k_j)g_{\mu\nu}. \tag{2}$$

The first term in Eq. (2) expresses the kinetic energy with m_i being mass of the valence quark; x_i and $\mathbf{k}_{\perp i}$ symbolize the longitudinal momentum fraction and transverse momentum carried by ith constituent of the system with $\sum_i x_i = 1$ and $\sum_i \mathbf{k}_{\perp i} = 0$. The second term in Eq. (2)

expresses the confining potential, which is separately defined in transverse and longitudinal directions through the soft-wall LF holographic QCD [84] and the phenomenological modeling [68], respectively. With regard to the compatibility of our harmonic oscillator (HO) basis function in the transverse direction (details about the basis are given in the ensuing paragraphs), the holographic QCD provides us with the HO potential. In the nonrelativistic limit, the total confinement potential emerges as a 3D HO potential [68,70,71,82]. The third term in Eq. (2) refers to the one gluon exchange interactions with coupling constant α_s, which underlies the dynamical spin structure in the LFWFs. Here, $u_{s_i}(k_i)$ represents the Dirac spinor with s_i and k_i being the spin and momentum carried by the ith valence quark. C_F and $g_{\mu\nu}$ define the color factor and the metric tensor, respectively. Further, the square of the average four-momentum transfer is expressed as $Q_{ij}^2 = -q^2 = -\frac{1}{2}((k_i' - k_i)^2 + (k_j' - k_j)^2)$.

Our goal is to follow BLFQ and evaluate the Hamiltonian, defined in Eq. (2), in a suitably truncated basis and diagonalize it to produce the baryon mass spectra and corresponding wave functions. For the BLFQ basis, we choose the 2D HO basis and the discretized plane-wave basis in transverse and longitudinal directions, respectively, to expand $|\Psi\rangle$ [65,66]. The orthonormalized 2D HO basis function in the transverse direction is given by

$$\phi_{n,m}(\mathbf{k}_\perp; b) = \frac{\sqrt{2}}{b(2\pi)^{3/2}} \sqrt{\frac{n!}{(n+|m|)!}} e^{-k_\perp^2/2b^2} \left(\frac{|k_\perp|}{b}\right)^{|m|} \\ \times L_n^{|m|}\left(\frac{k_\perp^2}{b^2}\right) e^{im\theta}, \tag{3}$$

where b is the HO scale parameter. The quantum numbers n and m represent the radial excitation and angular momentum projection, respectively, of a particle in a 2D HO. $L_n^{|m|}$ represents the associated Laguerre polynomial.

In the discretized plane-wave basis, the longitudinal momentum fraction of ith particle is represented by $x_i = \frac{p_i^+}{P^+} = \frac{k_i}{K}$ with the dimensionless quantity being $k = \frac{1}{2}, \frac{3}{2}, \frac{5}{2}, \cdots$ The values of k are chosen to signify the choice of antiperiodic boundary conditions. Note that $K = \sum_i k_i$. In addition, the total angular momentum projection is defined for many-body basis states as $M_J = \sum_i (m_i + \lambda_i)$ with λ being the quark helicity. The effective Hamiltonian in Eq. (2) conserves M_J, which leads to efficiencies in numerical calculations. We select $M_J = 1/2$ to solve for the proton spectroscopy.

Apart from restricting the Fock space, a further truncation is necessary to limit the basis size within each Fock sector. With our chosen basis, further truncation can be achieved by specifying two basis parameters (K) and (N_{max}). The former is conserved by the effective Hamiltonian, which is held fixed and controls the basis

in the longitudinal direction. Meanwhile, N_{max} limits a total transverse quantum number $N_\alpha = \sum_l (2n_l + |m_l| + 1)$ for multiparticle basis state $|\alpha\rangle$ such that $N_\alpha \leq N_{max}$. This parameter acts as a UV and an IR regulator for the LFWFs with $\Lambda_{UV} \approx b\sqrt{N_{max}}$ and $\Lambda_{IR} \approx b/\sqrt{N_{max}}$, respectively [66].

The resulting LFWFs in momentum space are expressed as

$$
\begin{aligned}
\Psi^\Lambda_{\{x_i, \mathbf{k}_{\perp i}, \lambda_i\}} &= \langle P, \Lambda | \{x_i, \mathbf{k}_{\perp i}, \lambda_i\} \rangle \\
&= \sum_{\{n_i, m_i\}} \left(\psi^\Lambda_{\{x_i, n_i, m_i, \lambda_i\}} \prod_i \phi_{n_i, m_i}(\mathbf{k}_{\perp i}; b) \right),
\end{aligned}
\tag{4}
$$

with $\psi^\Lambda_{\{x_i, n_i, m_i, \lambda_i\}} = \langle P, \Lambda | \{x_i, n_i, m_i, \lambda_i\} \rangle$ being the LFWF in BLFQ's chosen basis and with P and Λ being the momentum and helicity of the target spin-1/2 composite system, respectively.

To produce our LFWFs, the basis truncation parameters in the transverse and longitudinal directions are taken as $N_{max} = 10$ and $K = 16.5$, respectively [70,71]. Besides this, other model parameters are fixed in a way that they provide the known nucleon mass and the electromagnetic form factors [70,71], leading us to adopt $\{m_{q/\text{K.E.}}, m_{q/\text{OGE}}, \kappa, \alpha_s\} = \{0.3 \text{ GeV}, 0.2 \text{ GeV}, 0.34 \text{ GeV}, 1.1 \pm 0.1\}$ where

$m_{q/\text{K.E.}}$ and $m_{q/\text{OGE}}$ represent the quark masses in kinetic energy and OGE interaction terms with the HO scale parameter being $b = 0.6$ GeV. The calculated LFWFs for the valence Fock sector using these parameters, which imply a model scale $\mu_0^2 = 0.195 \pm 0.020$ GeV^2 [70,71], are employed to provide physical observables and distribution functions of the valence quarks inside the proton. In this work, we specifically study the proton GPDs using these LFWFs.

III. GENERALIZED PARTON DISTRIBUTIONS

The 3D spatial distributions are categorized as chiral-even and chiral-odd GPDs and are defined through the nonforward matrix elements of the bilocal operators between hadronic states. The connection between the correlator functions and various GPDs strictly depends upon the bilocal operator. Note that, for the present work, we restrict ourselves to the Dokshitzer-Gribov-Lipatov-Altarelli-Parisi region, $\zeta < x < 1$, where the number of partons in the initial and the final states remains conserved. Also, the momentum transfer in the longitudinal direction is taken to be zero. Accordingly, these distributions are classified and parametrized as we now show.

The distributions where the quark does not transfer helicity are parametrized as [85]

$$
\int \frac{dz^-}{8\pi} e^{\imath x P^+ z^-/2} \langle P', \Lambda' | \bar\varphi(0)\gamma^+ \varphi(z^-) | P, \Lambda \rangle |_{z^+ = \mathbf{z}_\perp = 0} = \frac{1}{2\bar{P}^+} \bar{u}(P', \Lambda') \left(H^q(x, \zeta, t)\gamma^+ + E^q(x, \zeta, t)\frac{\imath \sigma^{+\alpha}\Delta_\alpha}{2M_P} \right) u(P, \Lambda),
\tag{5}
$$

$$
\int \frac{dz^-}{8\pi} e^{\imath x P^+ z^-/2} \langle P', \Lambda' | \bar\varphi(0)\gamma^+\gamma_5 \varphi(z^-) | P, \Lambda \rangle |_{z^+ = \mathbf{z}_\perp = 0} = \frac{1}{2\bar{P}^+} \bar{u}(P', \Lambda') \left(\tilde{H}^q(x, \zeta, t)\gamma^+\gamma_5 + \tilde{E}^q(x, \zeta, t)\frac{\gamma_5\Delta^+}{2M_P} \right) u(P, \Lambda).
\tag{6}
$$

On the other hand, the transversity distributions where the quark transfers helicity are parametrized as [85]

$$
\begin{aligned}
&\int \frac{dz^-}{8\pi} e^{\imath x P^+ z^-/2} \langle P', \Lambda' | \bar\varphi(0)\sigma^{+j}\gamma_5 \varphi(z^-) | P, \Lambda \rangle |_{z^+ = \mathbf{z}_\perp = 0} \\
&= \frac{1}{2\bar{P}^+} \bar{u}(P', \Lambda') \left(H_T^q(x, \zeta, t)\sigma^{+j}\gamma_5 + \tilde{H}_T^q(x, \zeta, t)\frac{\epsilon^{+j\alpha\beta}\Delta_\alpha \bar{P}_\beta}{M_P^2} + E_T^q(x, \zeta, t)\frac{\epsilon^{+j\alpha\beta}\Delta_\alpha\gamma_\beta}{2M_P} + \tilde{E}_T^q(x, \zeta, t)\frac{\epsilon^{+j\alpha\beta}\bar{P}_\alpha\gamma_\beta}{M_P} \right) u(P, \Lambda),
\end{aligned}
\tag{7}
$$

with M_P being the mass of the target spin-1/2 composite system which is the proton in our case. We choose a frame such that the momenta of the target proton at the initial and final state, at $\zeta = 0$, become

$$
P = \left(P^+, \frac{M_P^2}{P^+}, \mathbf{0}_\perp \right),
\tag{8}
$$

$$
P' = \left(P^+, \frac{M_P^2 + \boldsymbol{\Delta}_\perp^2}{P^+}, -\boldsymbol{\Delta}_\perp \right).
\tag{9}
$$

where $\bar{P} = \frac{1}{2}(P + P')$. The overlap representation of the GPDs in terms of the LFWFs for $\zeta = 0$ are expressed as

$$
H^q(x, 0, t) = \sum_{\{\lambda_i\}} \int [d\mathcal{X} d\mathcal{K}_\perp] \Psi^{\uparrow *}_{\{x'_i, \mathbf{k}'_{\perp i}, \lambda_i\}} \Psi^{\uparrow}_{\{x_i, \mathbf{k}_{\perp i}, \lambda_i\}} \delta(x - x_1),
\tag{10}
$$

$$E^q(x,0,t) = -\frac{2M}{(\Delta^1 - \iota\Delta^2)}\sum_{\{\lambda_i\}}\int[\mathrm{d}\mathcal{X}\mathrm{d}\mathcal{K}_\perp]\Psi^{\uparrow*}_{\{x'_i,\mathbf{k}'_{\perp i},\lambda_i\}}\Psi^{\downarrow}_{\{x_i,\mathbf{k}_{\perp i},\lambda_i\}}\delta(x-x_1), \tag{11}$$

$$\tilde{H}^q(x,0,t) = \sum_{\{\lambda_i\}}\int[\mathrm{d}\mathcal{X}\mathrm{d}\mathcal{K}_\perp]\lambda_1\Psi^{\uparrow*}_{\{x'_i,\mathbf{k}'_{\perp i},\lambda_i\}}\Psi^{\uparrow}_{\{x_i,\mathbf{k}_{\perp i},\lambda_i\}}\delta(x-x_1), \tag{12}$$

$$E^q_T(x,0,t) + 2\tilde{H}^q_T(x,0,t) = \sum_{\{\lambda'_i,\lambda_i\}}\int[\mathrm{d}\mathcal{X}\mathrm{d}\mathcal{K}_\perp]\Psi^{\uparrow*}_{\{x'_i,\mathbf{k}'_{\perp i},\lambda'_i\}}\Psi^{\uparrow}_{\{x_i,\mathbf{k}_{\perp i},\lambda_i\}}\delta(x-x_1), \tag{13}$$

$$H^q_T(x,0,t) = \sum_{\{\lambda'_i,\lambda_i\}}\int[\mathrm{d}\mathcal{X}\mathrm{d}\mathcal{K}_\perp]\Psi^{\uparrow*}_{\{x'_i,\mathbf{k}'_{\perp i},\lambda'_i\}}\Psi^{\downarrow}_{\{x_i,\mathbf{k}_{\perp i},\lambda_i\}}\delta(x-x_1), \tag{14}$$

$$\tilde{H}^q_T(x,0,t) = -\sum_{\{\lambda'_i,\lambda_i\}}\int[\mathrm{d}\mathcal{X}\mathrm{d}\mathcal{K}_\perp]\Psi^{\downarrow*}_{\{x'_i,\mathbf{k}'_{\perp i},\lambda'_i\}}\Psi^{\uparrow}_{\{x_i,\mathbf{k}_{\perp i},\lambda_i\}}\delta_{\lambda_i,-\lambda'_i}\delta(x-x_1), \tag{15}$$

where

$$[\mathrm{d}\mathcal{X}\mathrm{d}\mathcal{K}_\perp] = \prod_{i=1}^{3}\frac{\mathrm{d}x_i\mathrm{d}^2\mathbf{k}_{\perp i}}{16\pi^3}16\pi^3\delta\left(1-\sum_{i=1}^{3}x_i\right)\delta^2\left(\sum_{i=1}^{3}\mathbf{k}_{\perp i}\right), \tag{16}$$

with the longitudinal momentum fraction and the transverse momentum for the active quark being $x'_1 = x_1$ and $\mathbf{k}'_{\perp 1} = \mathbf{k}_{\perp 1} + (1-x_1)\Delta_\perp$. For the spectators these momenta become $x'_i = x_i$ and $\mathbf{k}'_{\perp i} = \mathbf{k}_{\perp i} - x_i\Delta_\perp$. Here, $t = -\Delta_\perp^2$ when the skewness $\zeta = 0$.

We show the results of the chiral-even GPDs $(H, E, \tilde{H})$ for the valence quarks in Fig. 1, where the distribution functions are plotted with respect to the light-cone momentum (x) and the square of the total momentum transferred to the final proton state $(-t)$. The GPDs for u and d quarks are presented in the left and the right panels of Fig. 1, respectively. We find that the distributions have their maxima when the proton does not transfer transverse momentum to its final state and the struck quark inside the proton carries less than 50% of the proton's longitudinal momentum. As expected, by increasing the momentum transfer in the transverse direction, the distribution peak shifts gradually towards the higher values of x accompanied by a continuous drop in the magnitude. At the large x region, all the distributions eventually decay and become independent of t. However, this decay is observed to be faster for E^q than the other GPDs (H^q and $\tilde{H}^q$). As the anomalous magnetic moment and the axial charge are measured to be negative for the d quark, the connected GPDs, E^d and $\tilde{H}^d$, are correspondingly negative. All the mentioned features appear to be model independent as they have also been observed in other QCD inspired models [40–42,48,49,52].

When there is no momentum transfer $(t = 0)$, these distributions reproduce the valence quark distribution functions, particularly, the unpolarized and helicity-dependent functions, i.e., $H^q(x,0,0) = f^q(x)$ and $\tilde{H}^q(x,0,0) = g^q(x)$. These 1D functions have been studied previously in the BLFQ approach by considering both the Fock sector containing valence quarks ($|qqq\rangle$) [70,71] and one beyond this sector ($|qqqg\rangle$) [83]. Additionally, the detailed interpretation of the moments, which are functions of t, is given below in Sec. III A.

The 3D graphical representations of the chiral-odd proton GPDs $(H_T, E_T, \tilde{H}_T)$ for the u quark and the d quark are shown in the left and right panels of Fig. 2, respectively. Similar to the helicity conserving GPDs, these helicity nonconserving distribution functions are illustrated as functions of x and $-t$. All the helicity flip distributions show similar behavior as for the case of helicity nonflip GPDs, except the behavior of E^q_T and $\tilde{H}^q_T$ in the small x region. In that case, the peaks observed near $x \to 0$ are model dependent [43,51]. All the flavor distribution peaks move along x, when the momentum transfer from the initial proton is increased gradually. A noteworthy distribution is the combination of two chiral-odd GPDs, $2\tilde{H}^q_T + E^q_T$ which provides the details on the angular momentum contribution at certain limits and is reducible to the tensor form factor. We observe zero crossing points in E^d_T along x, which has also been observed in other models [43,51]. Our GPDs' results, for the case of H^u_T and $\tilde{H}^u_T$, are observed to be opposite to that of the d-quark distributions. Similar to H^q and $\tilde{H}^q$, the helicity nonconserving GPD H^q_T is reducible to transversity PDF, $H^q_T(x,0,0) = h^q(x)$ and has been previously studied in this approach [70,71,83].

We perform the QCD evolution to obtain the GPDs at higher scale μ^2 using the next-to-next-to-leading order Dokshitzer-Gribov-Lipatov-Altarelli-Paris equations of QCD [50,86–93]. To solve these equations numerically, we use the Higher Order Perturbative Parton Evolution
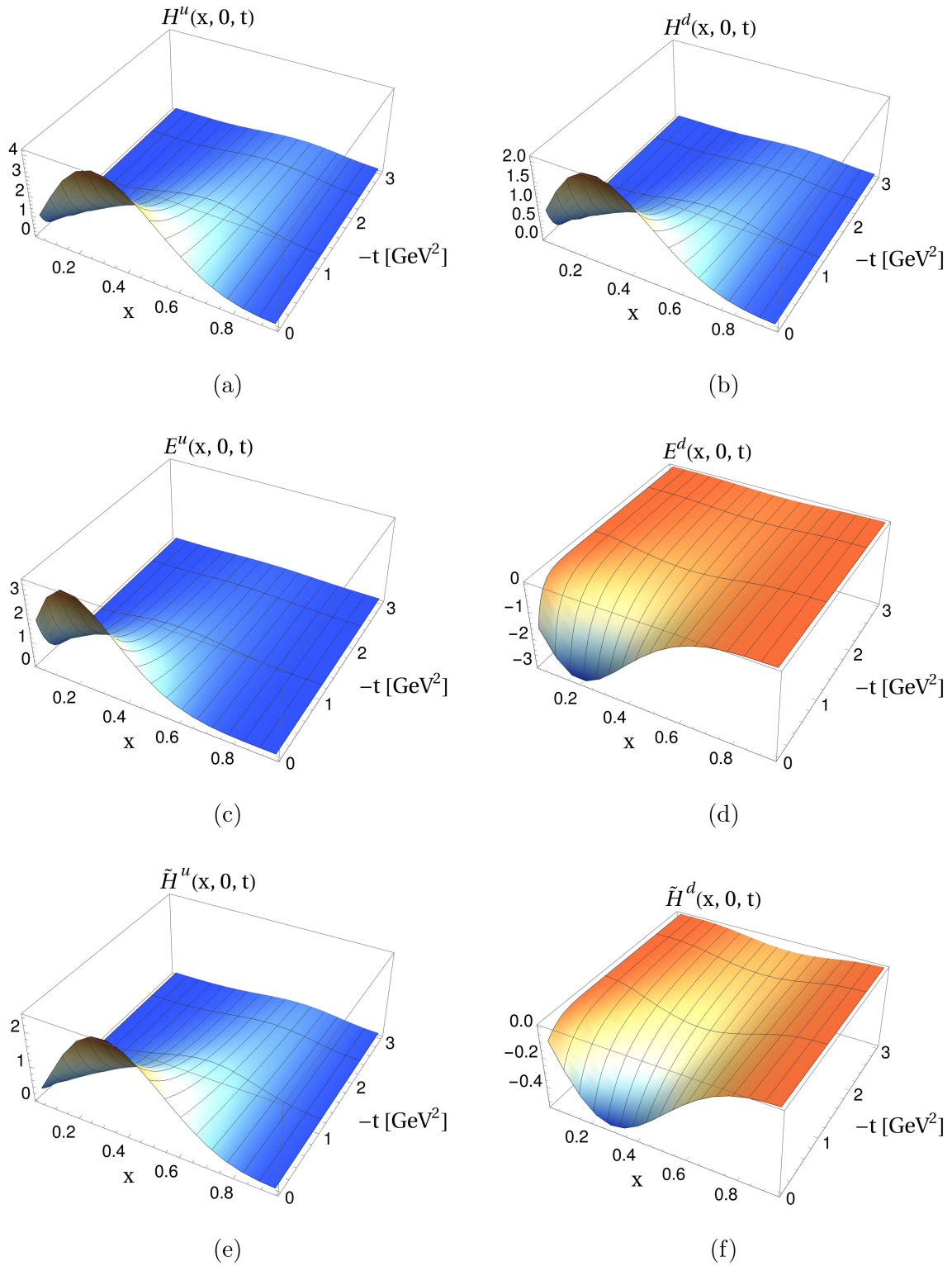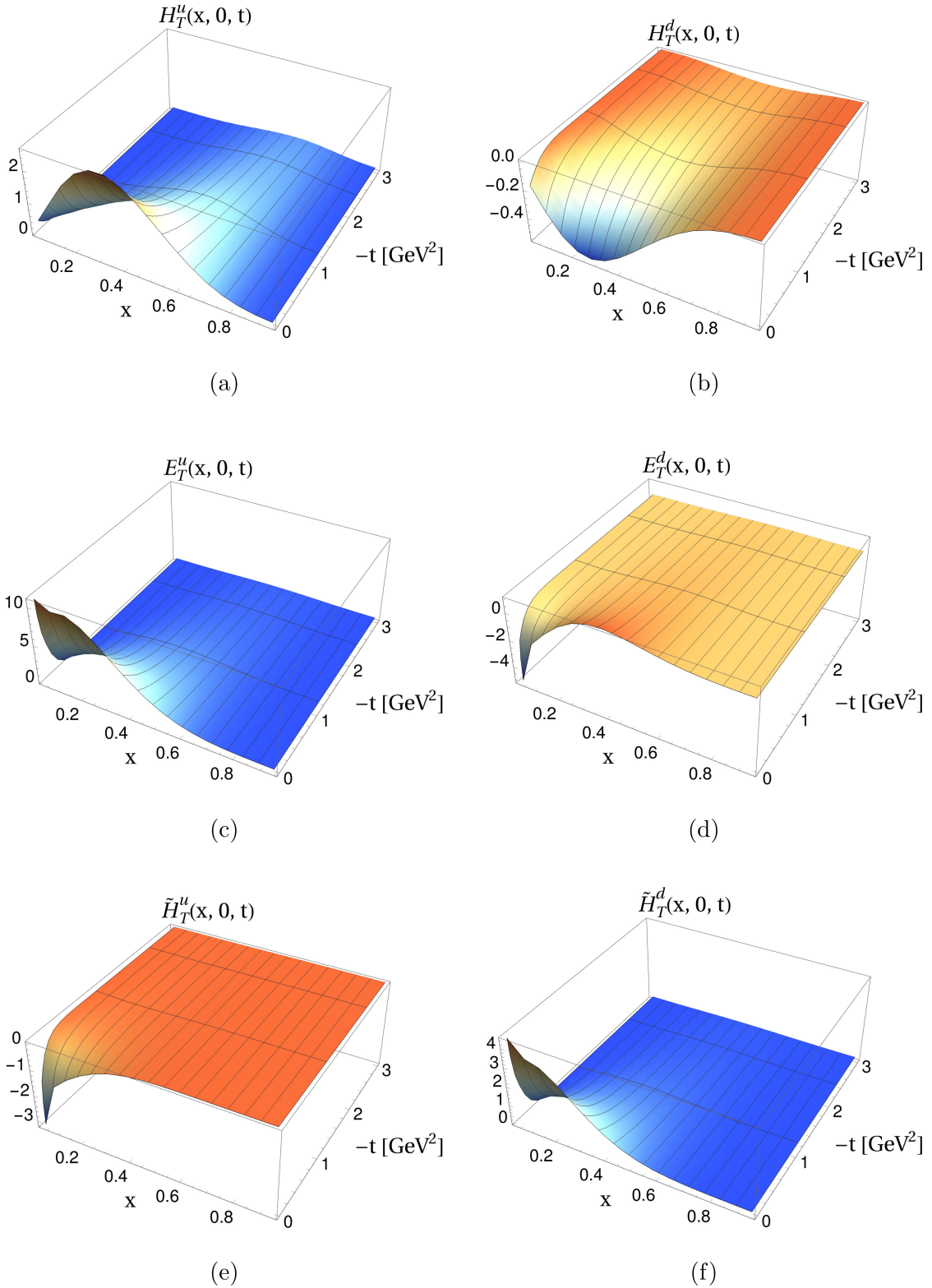
FIG. 1.   The chiral-even GPDs: (a) $H(x, 0, t)$, (c) $E(x, 0, t)$ and (e) $\tilde{H}(x, 0, t)$ for the u quark, where the respective GPDs for the d quark are shown in (b), (d), and (f). The GPDs are presented with respect to x and $-t$ (in GeV^2).

toolkit [94]. We show the evolved chiral-even GPDs, unpolarized GPD H^q and helicity GPD $\tilde{H}^q$, for both u and d quarks at different values of momentum transferred (t) in Fig. 3. The evolution is performed from the initial scale $\mu_0^2 = 0.195$ GeV^2 to $\mu^2 = 5$ GeV^2. The method is not well established for the evolution of transversity GPD; hence we refrain from evaluating this at the higher scale.

FIG. 2.   The chiral-odd GPDs (a) $H_T(x, 0, t)$, (c) $E_T(x, 0, t)$ and (e) $\tilde{H}_T(x, 0, t)$ for the u quark, where the respective GPDs for the d quark are shown in (b), (d), and (f). The GPDs are presented with respect to x and $-t$ (in GeV^2).
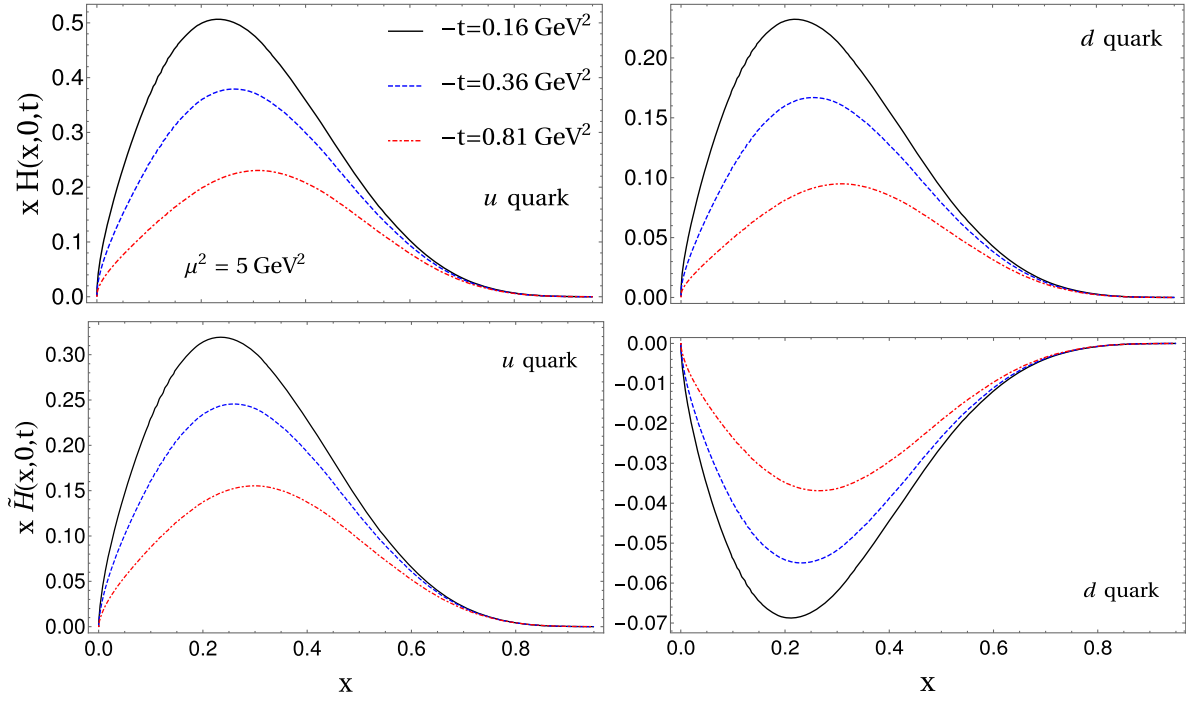
FIG. 3.   The GPDs H^q and $\tilde{H}^q$ multiplied by x evolved to the scale $\mu^2 = 5$ GeV^2 with respect to x.

(a)   (b)
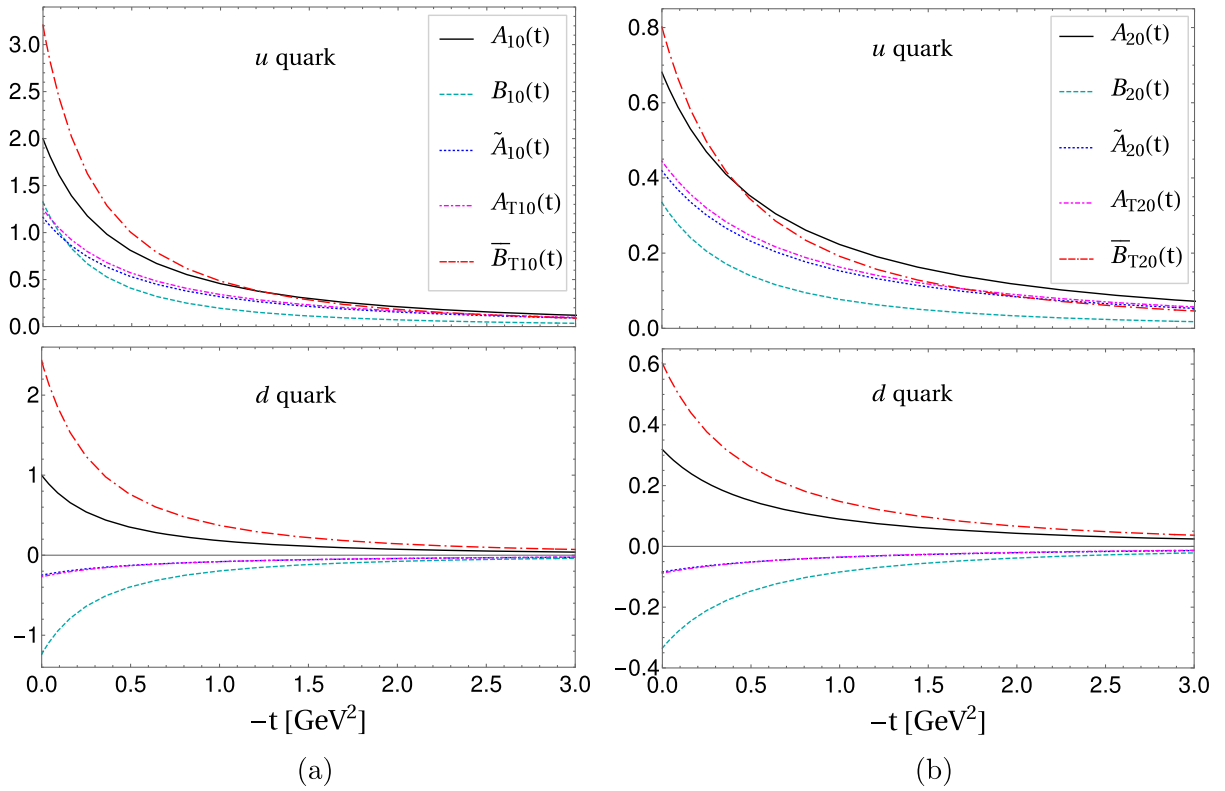
FIG. 4.   (a) The first and (b) second Mellin moments of GPDs, also known as generalized form factors, for the u quark (upper) and the d quark (lower) with respect to the square of the momentum transfer $-t$ (in GeV^2).
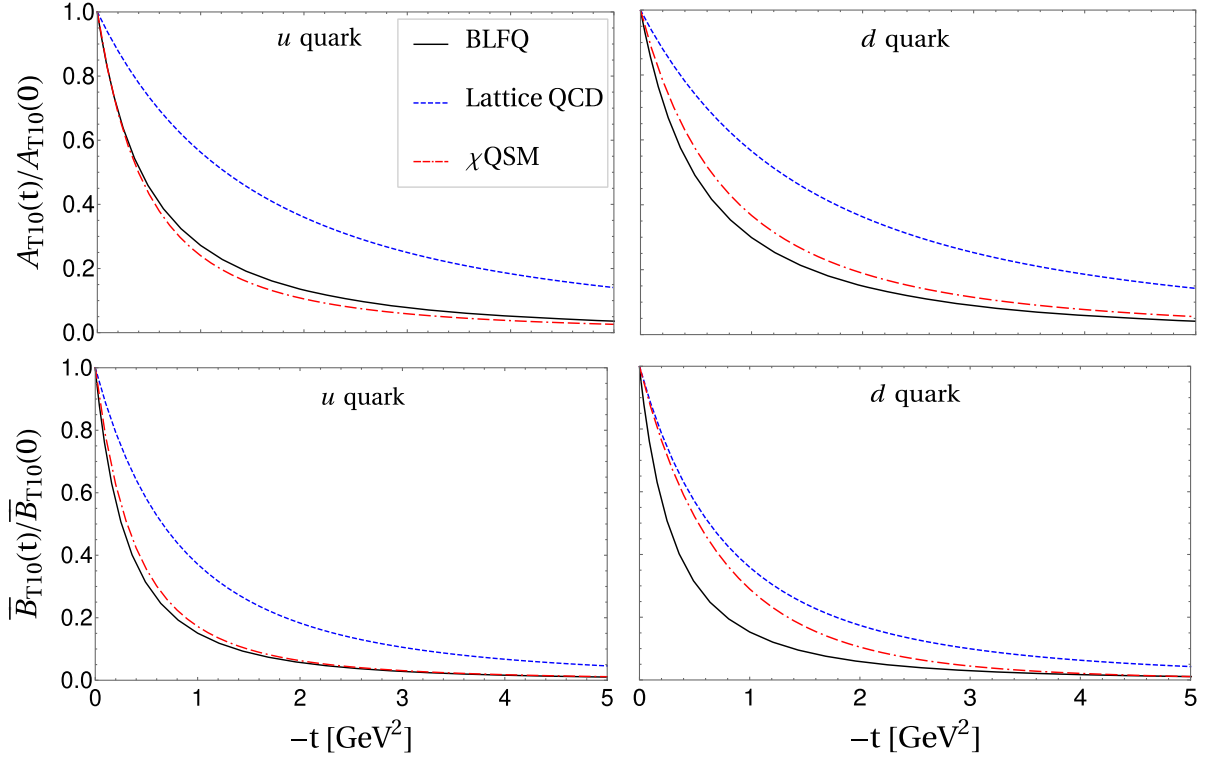
FIG. 5.   The normalized first Mellin moments with respect to $-t$ (in GeV^2) compared with the predictions of the lattice QCD approach [58,59] and the chiral quark soliton model (χQSM) [95,96].

A. Mellin moments of GPDs

For zero skewness ($\zeta = 0$), the moments of the valence quark GPDs are defined as

$$[\text{Mellin-moment}]_{n0}^q(t) = \int_0^1 dx\, x^{n-1}[\text{GPD}]^q(x,0,t), \quad (17)$$

where $n = 1, 2, 3, \ldots$ represent first, second, third moments and so on. The first moments of GPDs provide form factors depending upon the helicity configurations of the active quark and the proton. Specifically, the first moments of the unpolarized GPDs, $H^q(x, 0, t)$ and $E^q(x, 0, t)$, provide the Dirac and Pauli form factors, $F_1^q(t)$ and $F_2^q(t)$, respectively. The helicity-dependent GPDs, $\tilde{H}^q(x, 0, t)$ and $\tilde{E}^q(x, 0, t)$, give the axial-vector form factor $G_A^q(t)$ and the pseudo-scalar form factor $G_P^q(t)$, respectively. Lastly, the tensor form factors $g_T^q(t)$ and $\kappa_T^q(t)$ are provided by the chiral-odd GPDs. Mathematically,

$$F_1^q(t) = A_{10}^q(t) = \int dx H^q(x, 0, t),$$

$$F_2^q(t) = B_{10}^q(t) = \int dx E^q(x, 0, t), \quad (18)$$

$$G_A^q(t) = \tilde{A}_{10}^q(t) = \int dx \tilde{H}^q(x, 0, t),$$

$$G_P^q(t) = \tilde{B}_{10}^q(t) = \int dx \tilde{E}^q(x, 0, t), \quad (19)$$

$$g_T^q(t) = A_{T10}^q(t) = \int dx H_T^q(x, 0, t),$$

$$\kappa_T^q(t) = \bar{B}_{T10}^q(t) = \int dx [E_T^q(x, 0, t) + 2\tilde{H}_T^q(x, 0, t)], \quad (20)$$

and

$$A_{20}^q(t) = \int dx\, x H^q(x, 0, t), \quad B_{20}^q(t) = \int dx\, x E^q(x, 0, t), \quad (21)$$

$$\tilde{A}_{20}^q(t) = \int dx\, x \tilde{H}^q(x,0,t), \quad \tilde{B}_{20}^q(t) = \int dx\, x \tilde{E}^q(x,0,t), \quad (22)$$

$$A_{T20}^q(t) = \int dx\, x H_T^q(x, 0, t),$$

$$\bar{B}_{T20}^q(t) = \int dx\, x [E_T^q(x, 0, t) + 2\tilde{H}_T^q(x, 0, t)]. \quad (23)$$

TABLE I.   The values of first moment of the GPDs at $t = 0$ for u and d quarks in BLFQ.

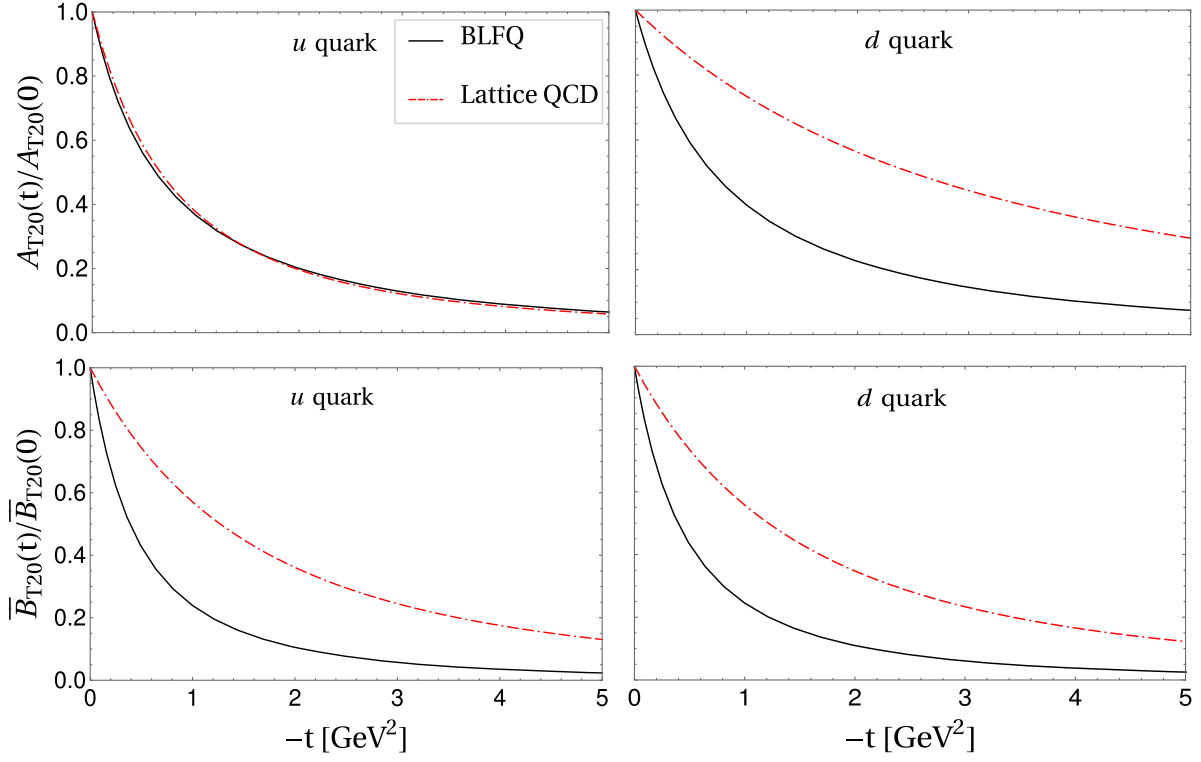| Quantity	$A_{10}(0)$	$B_{10}(0)$	$\tilde{A}_{10}(0)$	$A_{T10}(0)$	$\bar{B}_{T10}(0)$
u quark	2	1.367	1.162	1.251	3.208
d quark	1	-1.279	-0.249	-0.270	2.432

FIG. 6. The normalized second Mellin moments with respect to $-t$ (in GeV^2) compared with the predictions of the lattice QCD approach [58,59].

Now, in the forward limit ($t = 0$), the Dirac form factors exhibit the normalization as

$$F_1^u(0) = 2, \qquad F_1^d(0) = 1, \tag{24}$$

the Pauli form factors are regarded as the anomalous magnetic moments,

$$F_2^q(0) = \kappa^q, \tag{25}$$

the axial-vector form factors and pseudoscalar form factors are regarded as the axial-vector coupling constant (axial charge) and pseudoscalar coupling constant,

$$G_A^q(0) = g_A^q \quad \text{and} \quad G_P^q(0) = g_P^q, \tag{26}$$

respectively, and the tensor form factors identify with the tensor charge g_T^q and tensor magnetic moment κ_T^q.

In Fig. 4(a), we show the first Mellin moment of both chiral-even and chiral-odd GPDs, defined in Eqs. (18)–(20).
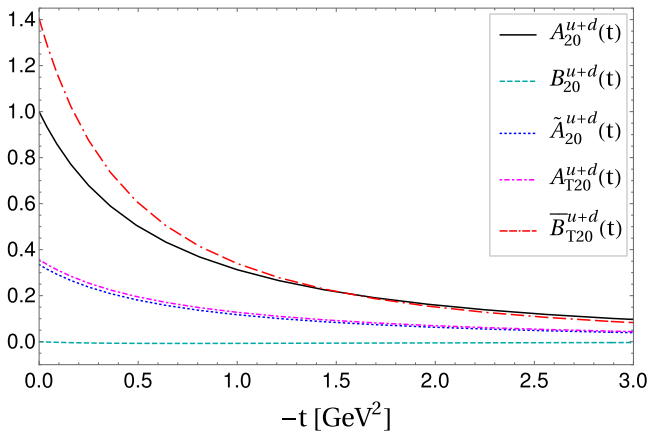
FIG. 7. The isoscalar generalized form factors with respect to the square of the momentum transfer $-t$ (in GeV^2).
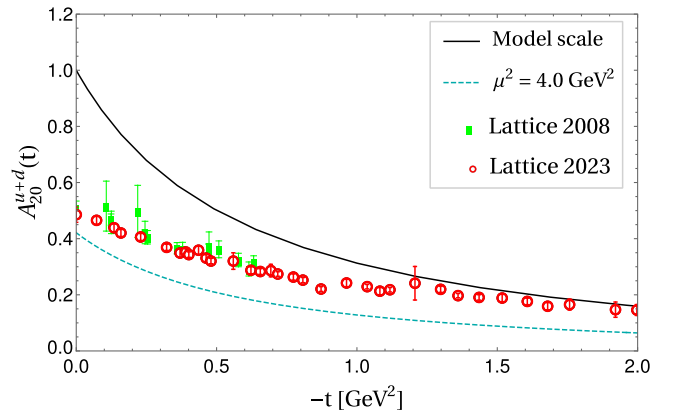
FIG. 8. The isoscalar generalized form factor A_{20} with respect to the square of the momentum transfer $-t$ (in GeV^2) in comparison with lattice QCD predictions [97,98].

TABLE II.　The values of second moment of the GPDs at $t = 0$ for u and d quarks in BLFQ.

Quantity	$A_{20}(0)$	$B_{20}(0)$	$\tilde{A}_{20}(0)$	$A_{T20}(0)$	$\bar{B}_{T20}(0)$
u-quark	0.681	0.335	0.419	0.445	0.802
d-quark	0.319	−0.335	−0.084	−0.088	0.604

TABLE III.　Our transversity asymmetry values for u quark and d quark in the proton compared with the predictions of the HO model [43], hypercentral CQM [43] and CQSM [101].

Transversity asymmetry	BLFQ	HO	Hypercentral CQM	CQSM
$\langle \delta^x J_u^x \rangle$	0.62	0.68	0.39	0.49
$\langle \delta^x J_d^x \rangle$	0.26	0.28	0.10	0.22

As discussed earlier, the first moment of unpolarized and helicity GPDs represent the Dirac, Pauli and axial form factors. The detailed study of these form factors can be found in Refs. [70,71], where reasonable agreement with the experimental data has been observed. Along with these form factors, we evaluate tensor form factors which are connected with A_{T10}^q and $\bar{B}_{T10}^q$.

The transversity GPDs are connected with the tensor FFs $A_{T10}^q (= g_T^q(t))$ and $\bar{B}_{T10}^q (= \kappa_T^q(t))$, and are illustrated in Fig. 4(a). When comparing with other published studies, we find that our tensor FFs qualitatively agree with the lattice QCD predictions for both u and d quarks [58,59] and with other model predictions [43,51,95,96]. We illustrate the t dependence of the first Mellin moments of chiral-odd GPDs, and compare our predictions with that of the lattice QCD approach [58,59] and the chiral quark soliton model (χQSM) [95,96] in Fig. 5. Since the lattice QCD method and the χQSM have predicted their results at 4 and 0.36 GeV^2, respectively, which are considerably different from our model scale $\mu_0^2 = 0.195 \pm 0.020$ GeV^2 [70,71], the comparison between them is only qualitative though

some similarities are apparent. Our model scale could be significantly increased when we increase our BLFQ basis spaces to include Fock components beyond the valence sector. We anticipate that, with these planned model improvements, our results may then become more comparable with the lattice QCD and other model predictions.

In Table I, we summarize our predictions for the first Mellin moments or the generalized form factors of the valence quark GPDs, when there is no momentum transfer from the initial to the final state of proton ($t = 0$). Similar to the other model results, we also observe that the tensor charge $g_T^q(0)(= A_{T10}^q)$ is larger than the axial charge $g_A^q(0)(= \tilde{A}_{10}^q(0))$, regardless of the sign. However, the difference is observed to be small in our BLFQ computation.

In Fig. 4(b), we present the second moment of the proton GPDs where, through a visual comparison to published lattice QCD results [58,59], we again find similarities in the qualitative behavior. To elucidate the comparison with lattice QCD results, we show the t dependence of the second Mellin moments of the chiral-odd GPDs in Fig. 6. Again, the predictions are made at different scales so that the comparison is only qualitative. The second moments give information about the gravitational form factors and our results for u and d quark contributions at $t = 0$ are shown in Table II. Further, by simply adding the second Mellin moments for u and d quarks, we obtain the isoscalar generalized FFs that we present in Fig. 7. Unlike other generalized FFs, B_{20}^{u+d} is observed to be independent of $-t$, and it appears to come out close to zero in our calculations. Furthermore, in Fig. 8, we have shown the comparison of our predictions of A_{20}^{u+d} by evolving it to the scale of the lattice QCD predictions [97,98], i.e. to $\mu^2 = 4$ GeV^2. A clear discrepancy has been observed which can be attributed to the fact that our calculations are based on only the leading Fock sector.

Since the GFFs $A_{20}(t)$ and $B_{20}(t)$ summing over all partons are scale invariant, we compare these GFFs in our BLFQ approach with those in the lattice QCD [98]
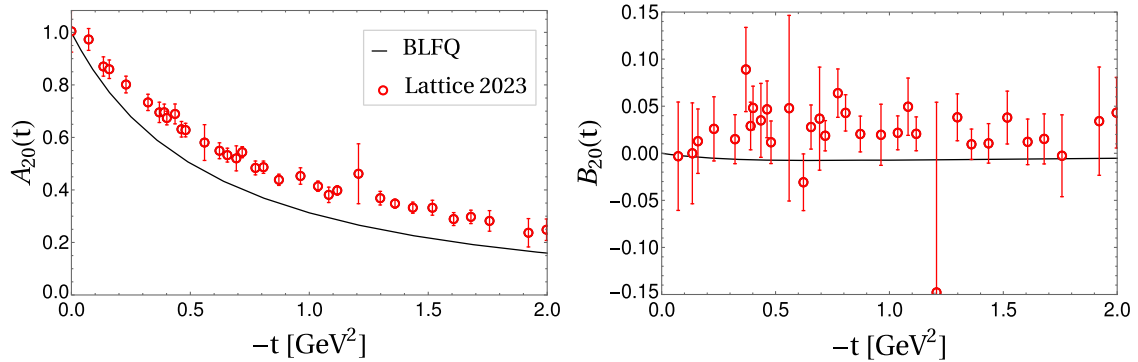
FIG. 9.　The form factors $A_{20}(t)$ and $B_{20}(t)$ with respect to the square of the momentum transfer $-t$ in comparison with lattice QCD predictions [98].
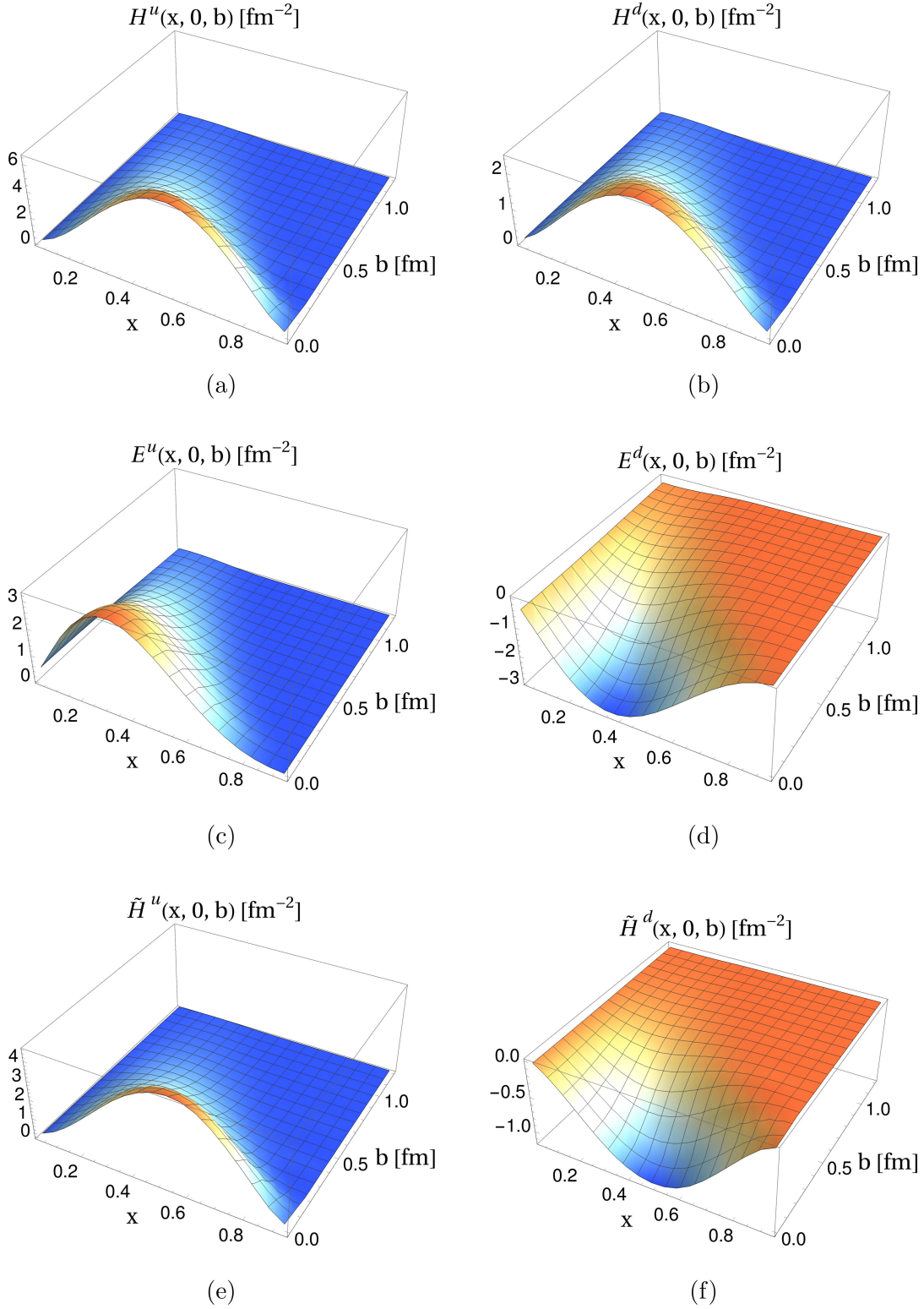
FIG. 10. The chiral-even GPDs: (a) $H(x, 0, b)$, (c) $E(x, 0, b)$ and (e) $\tilde{H}(x, 0, b)$ for the u quark, where the respective GPDs for the d quark are shown in (b), (d), and (f). The GPDs are presented with respect to x and b (in fm).
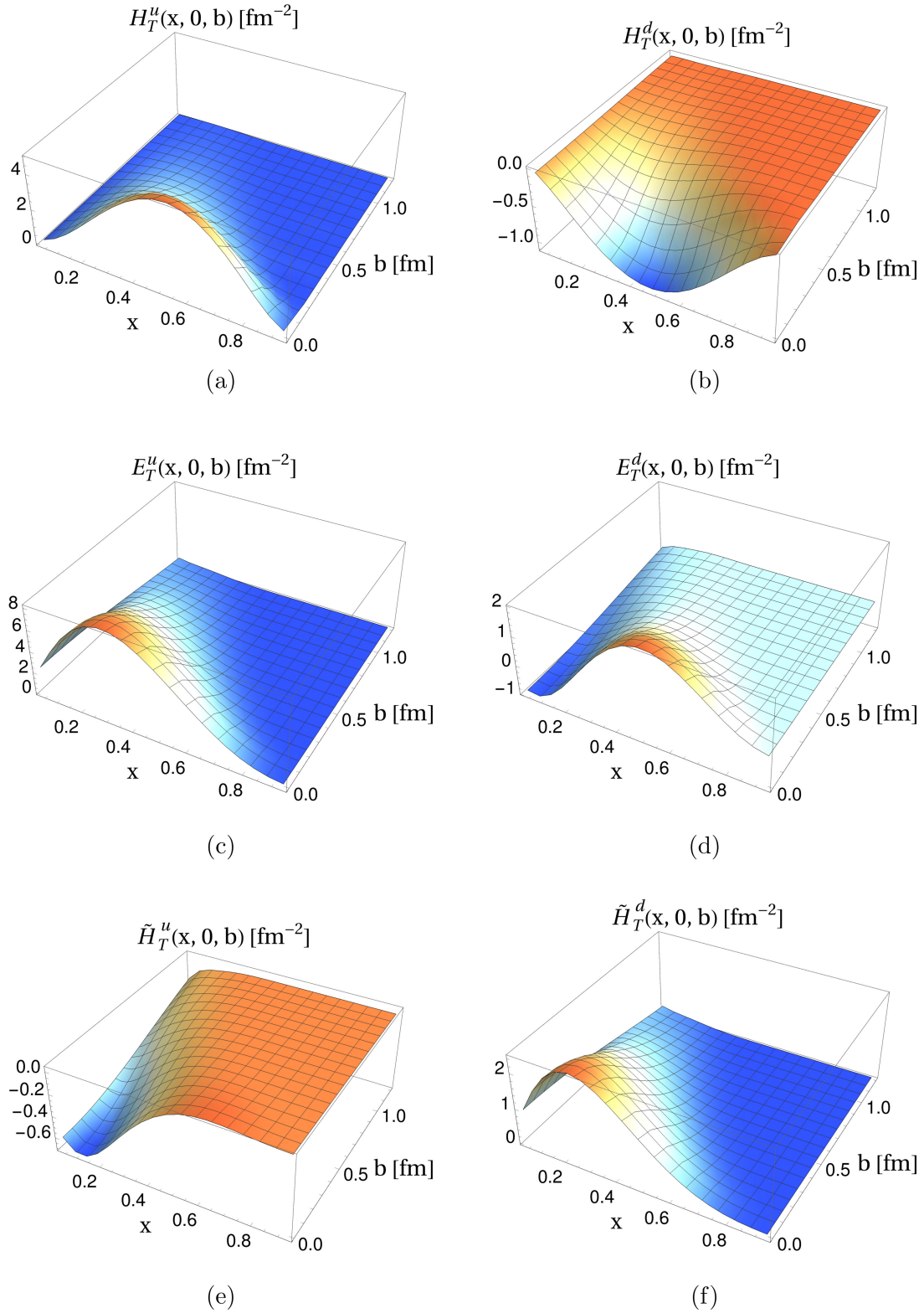
FIG. 11. The chiral-odd GPDs: (a) $H_T(x, 0, b)$, (c) $E_T(x, 0, b)$ and (e) $\tilde{H}_T(x, 0, b)$ for the u quark, where the respective GPDs for the d quark are shown in (b), (d), and (f). The GPDs are presented with respect to x and b (in fm).

in Fig. 9. Within our current treatment of the BLFQ approach, only u and d quarks contribute to these quantities, while the lattice QCD considers contribution from u, d, s quarks and gluons. We find that our results are somewhat underestimated compared to the lattice QCD predictions. This quantitative difference is expected as we consider only the valence Fock sector. On the other hand, the lattice QCD predictions involve first-principle calculations considering the quarks as well as the gluons. Our predictions may become closer to those of the lattice QCD when we explicitly include gluons and the sea quarks in our approach.

According to Ji sum rule, the second moment of the chiral-even GPDs give the partonic contribution to the total angular momentum of the proton [99], we have

$$J_q^z = \frac{1}{2} \int dx\, x [H^q(x,0,0) + E^q(x,0,0)]$$
$$= \frac{1}{2} [A_{20}^q(0) + B_{20}^q(0)]. \quad (27)$$

From Table II, we observe that Ji sum rule is satisfied in our model as we get $J_q^z = 1/2$ following Eq. (27). The detailed study on the total angular momentum contribution of the partons, when they do not flip their helicities, can be found in Ref. [80].

On the other hand, the second moments of chiral-odd GPDs are connected with the angular momentum carried by the partons with the transverse spin along the $\hat{x}$ direction in an unpolarized proton, J_q^x. According to Burkardt [100], this quantity is one half of the expectation value of the transversity asymmetry

$$\langle \delta^x J_q^x \rangle = \frac{1}{2} \int dx\, x [H_T^q(x,0,0) + 2\tilde{H}_T^q(x,0,0) + E_T^q(x,0,0)]$$
$$= \frac{1}{2} [A_{T20}^q(0) + \bar{B}_{T20}^q(0)]. \quad (28)$$

The obtained values of transversity asymmetry for u quarks and d quarks in our model as well as a comparison with other predictions from the HO model [43], hypercentral constituent quark model (CQM) [43] and chiral quark soliton model (CQSM) [101] are shown in Table III. We observe that our predictions are close to those of the HO model. Note that the methods chosen for comparison may have different initial scales, which could be a significant source of the differences in the results among the models.

B. Impact-parameter dependent GPDs

Taking the 2D Fourier transform of GPDs with respect to $\mathbf{\Delta}_\perp$ leads to the GPDs in transverse impact-parameter ($\mathbf{b}_\perp$) plane [1,2]. We have

$$[\text{GPD}](x,0,\mathbf{b}_\perp) = \frac{1}{(2\pi)^2} \int d^2\mathbf{\Delta}_\perp e^{-i\mathbf{\Delta}_\perp \cdot \mathbf{b}_\perp} [\text{GPD}](x,0,t),$$
$$= \frac{1}{2\pi} \int \Delta d\Delta J_0(\Delta b)[\text{GPD}](x,0,t), \quad (29)$$

where $\Delta = |\mathbf{\Delta}_\perp|$. The parameter $b = |\mathbf{b}_\perp|$ describes the transverse distance between the active quark and the center of momentum of the proton and satisfies the condition that $\sum_i x_i b_i = 0$, where the sum runs over the partons.

We show the unpolarized and helicity GPDs for the valence quarks as a function of x and b in Fig. 10. Furthermore, we present the 3D graphical representation of the transversity GPDs with respect to x and b in Fig. 11. We observe that all the GPDs, regardless of their signs, show a decrease in the width of the valence quark distributions in transverse impact-parameter plane, as x increases. For example, in Fig. 10(a), we find that the width decreases from 1.00 to 0.58 fm as x increases from 0.5 to 0.7. This implies that when the quarks take a larger longitudinal momentum fraction, they locate near the center of transverse position ($b = 0$). On the other hand, the peak of distributions shift towards the lower values of x accompanied by decreasing magnitude, and as we go away $b = 0$. Eventually, the distribution vanishes with increasing transverse distance. The rate of the dropoff varies for different GPDs, depending upon the helicities of both target proton and the active quark. All the GPDs have maximum distributions at $b = 0$. When the valence quarks carry more than 50% of the longitudinal momentum, the GPDs H^q, $\tilde{H}^q$ and H_T^q are observed to have this maxima, while the other GPDs have peaks at $x < 0.5$. Further, the flavor distributions E^d, $\tilde{H}^d$, H_T^d, $\tilde{H}_T^u$ are found negative. These signs in transverse b space are directly traced to the GPDs in momentum space (x, t). Our impact-parameter dependent GPDs show similarities with those of various studies in the literature [2,48,49,51,102–104], which leads us to suggest that there is an emerging trend towards model-independent characteristics.

IV. CONCLUSIONS

In this work, we have presented the leading-twist GPDs for the proton at zero skewness using the BLFQ approach, where the effective light-front Hamiltonian includes the transverse and longitudinal confinement as well as the one gluon exchange interaction between the valence quarks. The proton LFWFs have been obtained by treating it as a relativistic three-body system and by diagonalizing the effective Hamiltonian matrix numerically. The resulting LFWFs are utilized to study the various static and dynamic properties, relevant to the low-energy regime. The parameters used in this work were previously fixed to reproduce the proton mass and electromagnetic FFs [70,71].

The multidimensional GPDs, when taken to specific limits, represent unified versions of FFs and PDFs. We have

computed the chiral-even and chiral-odd nonskewed GPDs of the proton to observe the u and d quarks in momentum space, where we take into account the different configurations of helicities of both the active quark and target proton. We have found qualitatively similar behavior for the distributions at zero skewness to those in related studies [21,22,40–43,48,49,51,52]. Note that, we have not computed $\tilde{E}$ and $\tilde{E}_T$ as they require $\zeta \neq 0$ at the initial stage of evaluation in order to obtain the expressions which is beyond the scope of the present work. Further, these functions are capable of producing the different FFs based on the helicity dependence of both quark and the proton, such that the unpolarized, helicity and transversity GPDs provide Dirac, Pauli, axial and tensor FFs and are also known as the first Mellin moments of the GPDs. We observed that these FFs qualitatively match available predictions from other approaches [43,51,58,59,95,96]. We have also computed the second moments of the GPDs, which provide precise information on the gravitational form factors and are linked with the total angular momentum contributions of partons inside the proton. In addition, we have computed the GPDs in transverse position space. Again, we have found that our results show similar qualitative descriptions as obtained in other models.

Our approach can be systematically improved by incorporating Fock sectors beyond the valence quark component ($|qqq\rangle$). Our future efforts will include higher Fock components of the proton, for example, $|qqqq\bar{q}\rangle$, $|qqqg\rangle$ and so on. It will also be of great interest to see the distributions of sea quarks and gluons describing the proton structure with input from light-front QCD to the model at its initial scale.

ACKNOWLEDGMENTS

[1] M. Burkardt, Phys. Rev. D **62,** 071503 (2000); **66,** 119903(E) (2002).

[2] M. Burkardt, Int. J. Mod. Phys. A **18,** 173 (2003).

[3] V. D. Burkert, L. Elouadrhiri, and F. X. Girod, Nature (London) **557,** 396 (2018).

[4] X.-D. Ji, Phys. Rev. D **55,** 7114 (1997).

[5] A. V. Radyushkin, Phys. Rev. D **56,** 5524 (1997).

[6] A. V. Belitsky, D. Mueller, and A. Kirchner, Nucl. Phys. **B629,** 323 (2002).

[7] J. C. Collins, L. Frankfurt, and M. Strikman, Phys. Rev. D **56,** 2982 (1997).

[8] C. Adloff et al. (H1 Collaboration), Phys. Lett. B **517,** 47 (2001).

[9] A. Aktas et al. (H1 Collaboration), Eur. Phys. J. C **44,** 1 (2005).

[10] J. Breitweg et al. (ZEUS Collaboration), Eur. Phys. J. C **6,** 603 (1999).

[11] S. Chekanov et al. (ZEUS Collaboration), Phys. Lett. B **573,** 46 (2003).

[12] A. Airapetian et al. (HERMES Collaboration), Phys. Rev. Lett. **87,** 182001 (2001).

[13] A. Airapetian et al. (HERMES Collaboration), Phys. Rev. D **75,** 011103 (2007).

[14] A. Airapetian et al. (HERMES Collaboration), J. High Energy Phys. 06 (2008) 066.

[15] C. Muñoz Camacho et al. (Jefferson Lab Hall A and Hall A DVCS Collaborations), Phys. Rev. Lett. **97,** 262002 (2006).

[16] M. Mazouz et al. (Jefferson Lab Hall A Collaboration), Phys. Rev. Lett. **99,** 242501 (2007).

[17] S. Stepanyan *et al.* (CLAS Collaboration), Phys. Rev. Lett. **87**, 182002 (2001).

[18] S. Chen *et al.* (CLAS Collaboration), Phys. Rev. Lett. **97**, 072002 (2006).

[19] F. X. Girod *et al.* (CLAS Collaboration), Phys. Rev. Lett. **100**, 162002 (2008).

[20] N. d'Hose, E. Burtin, P. A. M. Guichon, and J. Marroncle, Eur. Phys. J. A **19**, 47 (2004).

[21] H. Hashamipour, M. Goharipour, K. Azizi, and S. V. Goloskokov, Phys. Rev. D **105**, 054002 (2022).

[22] H. Hashamipour, M. Goharipour, and S. S. Gousheh, Phys. Rev. D **102**, 096014 (2020).

[23] D. Y. Ivanov, B. Pire, L. Szymanowski, and O. V. Teryaev, Phys. Lett. B **550**, 65 (2002).

[24] R. Enberg, B. Pire, and L. Szymanowski, Eur. Phys. J. C **47**, 87 (2006).

[25] M. El Beiyad, B. Pire, M. Segond, L. Szymanowski, and S. Wallon, Phys. Lett. B **688**, 154 (2010).

[26] S. Ahmad, G. R. Goldstein, and S. Liuti, Phys. Rev. D **79**, 054014 (2009).

[27] S. V. Goloskokov and P. Kroll, Eur. Phys. J. C **65**, 137 (2010).

[28] S. V. Goloskokov and P. Kroll, Eur. Phys. J. A **47**, 112 (2011).

[29] G. R. Goldstein, J. O. Gonzalez Hernandez, and S. Liuti, J. Phys. G **39**, 115001 (2012).

[30] G. R. Goldstein, J. O. Gonzalez Hernandez, and S. Liuti, Phys. Rev. D **91**, 114013 (2015).

[31] P. Kroll, Few-Body Syst. **57**, 1041 (2016).

[32] C. Adolph *et al.* (COMPASS Collaboration), Phys. Lett. B **731**, 19 (2014).

[33] I. Bedlinskiy *et al.* (CLAS Collaboration), Phys. Rev. Lett. **109**, 112001 (2012).

[34] V. Kubarovsky (CLAS Collaboration), Int. J. Mod. Phys. Conf. Ser. **40**, 1660051 (2016).

[35] R. Abdul Khalek *et al.*, Nucl. Phys. **A1026**, 122447 (2022).

[36] D. P. Anderle *et al.*, Front. Phys. (Beijing) **16**, 64701 (2021).

[37] X. Cao and J. Zhang, Eur. Phys. J. C **83**, 505 (2023).

[38] J. Dudek *et al.*, Eur. Phys. J. A **48**, 187 (2012).

[39] V. D. Burkert, Annu. Rev. Nucl. Part. Sci. **68**, 405 (2018).

[40] X.-D. Ji, W. Melnitchouk, and X. Song, Phys. Rev. D **56**, 5511 (1997).

[41] S. Boffi, B. Pasquini, and M. Traini, Nucl. Phys. **B649**, 243 (2003).

[42] S. Boffi, B. Pasquini, and M. Traini, Nucl. Phys. **B680**, 147 (2004).

[43] B. Pasquini, M. Pincetti, and S. Boffi, Phys. Rev. D **72**, 094029 (2005).

[44] S. Scopetta and V. Vento, Phys. Rev. D **71**, 014014 (2005).

[45] K. Goeke, M. V. Polyakov, and M. Vanderhaeghen, Prog. Part. Nucl. Phys. **47**, 401 (2001).

[46] M. Penttinen, M. V. Polyakov, and K. Goeke, Phys. Rev. D **62**, 014024 (2000).

[47] V. Y. Petrov, P. V. Pobylitsa, M. V. Polyakov, I. Bornig, K. Goeke, and C. Weiss, Phys. Rev. D **57**, 4325 (1998).

[48] C. Mondal and D. Chakrabarti, Eur. Phys. J. C **75**, 261 (2015).

[49] C. Mondal, Eur. Phys. J. C **77**, 640 (2017).

[50] T. Maji, C. Mondal, and D. Chakrabarti, Phys. Rev. D **96**, 013006 (2017).

[51] D. Chakrabarti and C. Mondal, Phys. Rev. D **92**, 074012 (2015).

[52] A. Freese and I. C. Cloët, Phys. Rev. C **103**, 045204 (2021).

[53] S. Bhattacharya, K. Cichy, M. Constantinou, J. Dodson, X. Gao, A. Metz, S. Mukherjee, A. Scapellato, F. Steffens, and Y. Zhao, Phys. Rev. D **106**, 114512 (2022).

[54] C. Alexandrou, K. Cichy, M. Constantinou, K. Hadjiyiannakou, K. Jansen, A. Scapellato, and F. Steffens, Phys. Rev. D **105**, 034501 (2022).

[55] C. Alexandrou *et al.*, Phys. Rev. D **107**, 054504 (2023).

[56] Y. Guo, X. Ji, and K. Shiells, J. High Energy Phys. 09 (2022) 215.

[57] C. Alexandrou, K. Cichy, M. Constantinou, K. Hadjiyiannakou, K. Jansen, A. Scapellato, and F. Steffens, Phys. Rev. Lett. **125**, 262001 (2020).

[58] M. Gockeler, P. Hagler, R. Horsley, D. Pleiter, P. E. L. Rakow, A. Schafer, G. Schierholz, and J. M. Zanotti (QCDSF and UKQCD Collaborations), Phys. Lett. B **627**, 113 (2005).

[59] M. Göckeler, P. Hägler, R. Horsley, Y. Nakamura, D. Pleiter, P. E. L. Rakow, A. Schäfer, G. Schierholz, H. Stüben, and J. M. Zanotti (QCDSF and UKQCD Collaborations), Phys. Rev. Lett. **98**, 222001 (2007).

[60] C. Alexandrou *et al.*, Phys. Rev. D **101**, 034519 (2020).

[61] C. Chen and C. D. Roberts, Eur. Phys. J. A **58**, 206 (2022).

[62] S.-S. Xu, C. Chen, I. C. Cloet, C. D. Roberts, J. Segovia, and H.-S. Zong, Phys. Rev. D **92**, 114034 (2015).

[63] C. Chen, C. S. Fischer, C. D. Roberts, and J. Segovia, Phys. Lett. B **815**, 136150 (2021).

[64] Z.-F. Cui, C. Chen, D. Binosi, F. de Soto, C. D. Roberts, J. Rodríguez-Quintero, S. M. Schmidt, and J. Segovia, Phys. Rev. D **102**, 014043 (2020).

[65] J. P. Vary, H. Honkanen, J. Li, P. Maris, S. J. Brodsky, A. Harindranath, G. F. de Teramond, P. Sternberg, E. G. Ng, and C. Yang, Phys. Rev. C **81**, 035205 (2010).

[66] X. Zhao, H. Honkanen, P. Maris, J. P. Vary, and S. J. Brodsky, Phys. Lett. B **737**, 65 (2014).

[67] P. Wiecki, Y. Li, X. Zhao, P. Maris, and J. P. Vary, Phys. Rev. D **91**, 105009 (2015).

[68] Y. Li, P. Maris, X. Zhao, and J. P. Vary, Phys. Lett. B **758**, 118 (2016).

[69] Y. Li, P. Maris, and J. P. Vary, Phys. Rev. D **96**, 016022 (2017).

[70] C. Mondal, S. Xu, J. Lan, X. Zhao, Y. Li, D. Chakrabarti, and J. P. Vary, Phys. Rev. D **102**, 016008 (2020).

[71] S. Xu, C. Mondal, J. Lan, X. Zhao, Y. Li, and J. P. Vary (BLFQ Collaboration), Phys. Rev. D **104**, 094036 (2021).

[72] S. Nair, C. Mondal, X. Zhao, A. Mukherjee, and J. P. Vary (BLFQ Collaboration), Phys. Lett. B **827**, 137005 (2022).

[73] J. Lan, C. Mondal, S. Jia, X. Zhao, and J. P. Vary, Phys. Rev. Lett. **122**, 172001 (2019).

[74] S. Jia and J. P. Vary, Phys. Rev. C **99**, 035206 (2019).

[75] S. Tang, Y. Li, P. Maris, and J. P. Vary, Phys. Rev. D **98**, 114038 (2018).

[76] J. Lan, C. Mondal, S. Jia, X. Zhao, and J. P. Vary, Phys. Rev. D **101**, 034024 (2020).

[77] J. Lan, C. Mondal, M. Li, Y. Li, S. Tang, X. Zhao, and J. P. Vary, Phys. Rev. D **102**, 014020 (2020).

[78] L. Adhikari, C. Mondal, S. Nair, S. Xu, S. Jia, X. Zhao, and J. P. Vary (BLFQ Collaboration), Phys. Rev. D **104**, 114019 (2021).

[79] J. Lan, K. Fu, C. Mondal, X. Zhao, and J. P. Vary (BLFQ Collaboration), Phys. Lett. B **825**, 136890 (2022).

[80] Y. Liu, S. Xu, C. Mondal, X. Zhao, and J. P. Vary (BLFQ Collaboration), Phys. Rev. D **105**, 094018 (2022).

[81] T. Peng, Z. Zhu, S. Xu, X. Liu, C. Mondal, X. Zhao, and J. P. Vary (BLFQ Collaboration), Phys. Rev. D **106**, 114040 (2022).

[82] Z. Hu, S. Xu, C. Mondal, X. Zhao, and J. P. Vary (BLFQ Collaboration), Phys. Lett. B **833**, 137360 (2022).

[83] S. Xu, C. Mondal, X. Zhao, Y. Li, and J. P. Vary, arXiv: 2209.08584.

[84] S. J. Brodsky, G. F. de Teramond, H. G. Dosch, and J. Erlich, Phys. Rep. **584**, 1 (2015).

[85] M. Diehl, Phys. Rep. **388**, 41 (2003).

[86] Y. L. Dokshitzer, Sov. Phys. JETP **46**, 641 (1977).

[87] V. N. Gribov and L. N. Lipatov, Sov. J. Nucl. Phys. **15**, 438 (1972).

[88] G. Altarelli and G. Parisi, Nucl. Phys. **B126**, 298 (1977).

[89] A. V. Belitsky, B. Geyer, D. Mueller, and A. Schafer, Phys. Lett. B **421**, 312 (1998).

[90] A. Freund and M. F. McDermott, Phys. Rev. D **65**, 056012 (2002); **66**, 079903(E) (2002).

[91] S. Scopetta and V. Vento, Phys. Rev. D **69**, 094004 (2004).

[92] M. Diehl, T. Feldmann, R. Jakob, and P. Kroll, Eur. Phys. J. C **39**, 1 (2005).

[93] M. Diehl and W. Kugler, Phys. Lett. B **660**, 202 (2008).

[94] G. P. Salam and J. Rojo, Comput. Phys. Commun. **180**, 120 (2009).

[95] T. Ledwig, A. Silva, and H.-C. Kim, Phys. Rev. D **82**, 034022 (2010).

[96] T. Ledwig and H.-C. Kim, Phys. Rev. D **85**, 034041 (2012).

[97] P. Hagler et al. (LHPC Collaboration), Phys. Rev. D **77**, 094502 (2008).

[98] D. C. Hackett, D. A. Pefkou, and P. E. Shanahan, arXiv: 2310.08484.

[99] X.-D. Ji, Phys. Rev. Lett. **78**, 610 (1997).

[100] M. Burkardt, Phys. Rev. D **72**, 094020 (2005).

[101] M. Wakamatsu, Phys. Rev. D **79**, 014033 (2009).

[102] H. Dahiya and A. Mukherjee, Phys. Rev. D **77**, 045032 (2008).

[103] D. Chakrabarti and C. Mondal, Phys. Rev. D **88**, 073006 (2013).

[104] A. Vega, I. Schmidt, T. Gutsche, and V. E. Lyubovitskij, Phys. Rev. D **83**, 036001 (2011).